Acoustooptic characterization of a birefringent two-mode photonic crystal fiber

Magnus W. Haakestad and Helge E. Engan

Department of Electronics and Telecommunications
Norwegian University of Science and Technology, NO-7491 Trondheim, Norway
Magnus-W.Haakestad@ffi.no

Abstract: The effect of axial variations in acoustooptic phase-mismatch coefficient of a two-mode birefringent photonic crystal fiber (PCF) is studied experimentally using two different methods. The first method is to determine axial non-uniformities directly from the transmission spectrum, while the second method is to use acoustic pulses. Both methods are seen to be in good agreement. It is found that axial non-uniformities increase the coupling bandwidth significantly as compared to an axially uniform fiber. The effect of acoustic birefringence is also considered.

© 2006 Optical Society of America

References and links

1. H. S. Kim, S. H. Yun, I. K. Kwang, and B. Y. Kim, "All-fiber acousto-optic tunable notch filter with electronically controllable spectral profile," Opt. Lett. **22**, 1476–1478 (1997).
2. B. Y. Kim, J. N. Blake, H. E. Engan, and H. J. Shaw, "All-fiber acousto-optic frequency shifter," Opt. Lett. **11**, 389–391 (1986).
3. H. E. Engan, B. Y. Kim, J. N. Blake, and H. J. Shaw, "Propagation and Optical Interaction of Guided Acoustic Waves in Two-Mode Optical Fibers," J. Lightwave Technol. **6**, 428–436 (1988).
4. S. Ramachandran, "Dispersion-Tailored Few-Mode Fibers: A Versatile Platform for In-Fiber Photonic Devices," J. Lightwave Technol. **23**, 3426–3443 (2005).
5. T. Jin, Q. Li, J. Zhao, K. Cheng, and X. Liu, "Ultra-Broad-Band AOTF Based on Cladding Etched Single-Mode Fiber," IEEE Photon. Technol. Lett. **14**, 1133–1135 (2002).
6. Q. Li, A. A. Au, C.-H. Lin, E. R. Lyons, and H. P. Lee, "An Efficient All-Fiber Variable Optical Attenuator via Acoustooptic Mode Coupling," IEEE Photon. Technol. Lett. **14**, 1563–1565 (2002).
7. D. Östling and H. E. Engan, "Narrow-band acousto-optic tunable filtering in a two-mode fiber," Opt. Lett. **20**, 1247–1249 (1995).
8. T. E. Dimmick, G. Kakarantzas, T. A. Birks, A. Diez, and P. S. J. Russell, "Compact All-Fiber Acoustooptic Tunable Filters with Small Bandwidth-Length Product," IEEE Photon. Technol. Lett. **12**, 1210–1212 (2000).
9. Q. Li, X. Liu, and H. P. Lee, "Demonstration of Narrow-Band Acoustooptic Tunable Filters on Dispersion-Enhanced Single-Mode Fibers," IEEE Photon. Technol. Lett. **14**, 1551–1553 (2002).
10. D. I. Yeom, H. S. Kim, M. S. Kang, H. S. Park, and B. Y. Kim, "Narrow-Bandwidth All-Fiber Acoustooptic Tunable Filter With Low Polarization-Sensitivity," IEEE Photon. Technol. Lett. **17**, 2646–2648 (2005).
11. J. Broeng, D. Mogilevstev, S. E. Barkou, and A. Bjarklev, "Photonic Crystal Fibers: A New Class of Optical Waveguides," Opt. Fiber Technol. **5**, 305–330 (1999).
12. P. Russell, "Photonic Crystal Fibers," Science **299**, 358–362 (2003).
13. A. Diez, T. A. Birks, W. H. Reeves, B. J. Mangan, and P. S. J. Russell, "Excitation of cladding modes in photonic crystal fibers by flexural acoustic waves," Opt. Lett. **25**, 1499–1501 (2000).
14. M. W. Haakestad and H. E. Engan, "Acoustooptic Properties of a Weakly Multimode Solid Core Photonic Crystal Fiber," J. Lightwave Technol. **24**, 838–845 (2006).

15. B. Y. Kim, J. N. Blake, S. Y. Huang, and H. J. Shaw, "Use of highly elliptical core fibers for two-mode fiber devices," Opt. Lett. **12**, 729–731 (1987).
16. W. Jin, Z. Wang, and J. Ju, "Two-mode photonic crystal fibers," Opt. Express **13**, 2082–2088 (2005).
17. W. R. Trutna, Jr., D. W. Dolfi, and C. A. Flory, "Anomalous sidelobes and birefringence apodization in acousto-optic tunable filters," Opt. Lett. **18**, 28–30 (1993).
18. D. A. Smith, A. d'Alessandro, J. E. Baran, and H. Herrmann, "Source of sidelobe asymmetry in integrated acousto-optic filters," Appl. Phys. Lett. **62**, 814–816 (1993).
19. B. Langli, D. Östling, and K. Bløtekjær, "Axial Variations in the Acoustooptic Phase-Mismatch Coefficient of Two-Mode Fibers," J. Lightwave Technol. **16**, 2443–2450 (1998).
20. R. W. Gerchberg and W. O. Saxton, "A Practical Algorithm for the Determination of Phase from Image and Diffraction Plane Pictures," Optik **35**, 237–246 (1972).
21. J. Skaar and H. E. Engan, "Distributed intragrating sensing using phase retrieval," Proc. SPIE **3746**, 588–591 (1999).
22. A. Ortigosa-Blanch, J. C. Knight, W. J. Wadsworth, J. Arriaga, B. J. Mangan, T. A. Birks, and P. S. J. Russell, "Highly birefringent photonic crystal fibers," Opt. Lett. **25**, 1325–1327 (2000).
23. T. P. Hansen, J. Broeng, S. E. B. Libori, E. Knudsen, A. Bjarklev, J. R. Jensen, and H. Simonsen, "Highly Birefringent Index-Guiding Photonic Crystal Fibers," IEEE Photon. Technol. Lett. **13**, 588–590 (2001).
24. K. Suzuki, H. Kubota, S. Kawanishi, M. Tanaka, and M. Fujita, "High-speed bi-directional polarisation division multiplexed optical transmission in ultra low-loss (1.3 dB/km) polarisation-maintaining photonic crystal fibre," Electron. Lett. **37**, 1399–1401 (2001).
25. J. R. Folkenberg, M. D. Nielsen, N. A. Mortensen, C. Jakobsen, and H. R. Simonsen, "Polarization maintaining large mode area photonic crystal fiber," Opt. Express **12**, 956–960 (2004).
26. S. G. Johnson and J. D. Joannopoulos, "Block-iterative frequency-domain methods for Maxwell's equations in a planewave basis," Opt. Express **8**, 173–190 (2001).
27. R. Feced, C. Alegria, M. N. Zervas, and R. I. Laming, "Acoustooptic Attenuation Filters Based on Tapered Optical Fibers," IEEE J. Sel. Top. Quantum Electron. **5**, 1278–1288 (1999).
28. H. E. Engan, D. Östling, P. O. Kval, and J. O. Askautrud, "Wideband operation of horns for excitation of acoustic modes in optical fibers," Proc. SPIE **2360**, 568–571 (1994).
29. B. Langli and K. Bløtekjær, "Effect of Acoustic Birefringence on Acoustooptic Interaction in Birefringent Two-Mode Optical Fibers," J. Lightwave Technol. **21**, 528–535 (2003).
30. J. O. Askautrud and H. E. Engan, "Distributed probing of the orientation of two-mode birefringent fiber using pulsed acoustic guided waves," Proc. SPIE **1267**, 40–49 (1990).

1. Introduction

Acoustooptic (AO) coupling in optical fibers has been applied to the design of many devices, such as tunable filters [1]. These devices rely on coupling between two optical modes, induced by a traveling acoustic wave acting as a long period grating [2,3]. By tailoring fiber parameters, it is possible to make broadband and narrow-band filters [4–10].

There exists a new class of optical fibers, called photonic crystal fibers (also denoted micro-structured optical fibers or holey optical fibers) [11,12], which offer a large degree of freedom in tailoring fiber parameters. Previously, acoustooptic coupling between the fundamental mode and a cladding mode, as well as coupling between the fundamental mode and weakly guided second order modes has been demonstrated in index-guiding PCFs [13,14]. In Ref. [14] it was found that the coupling bandwidth was larger than expected for coupling to a single mode in a uniform fiber, and it was pointed out that this was likely due to the combined effect of splitting in mode index between the nearly degenerate higher order modes and axial non-uniformities. The four nearly degenerate higher order modes are reduced to two pairs of linearly polarized second order modes with stable lobe orientations in birefringent fibers [15,16]. This enables selective excitation of the higher order modes and avoids the problem of coupling to several nearly degenerate modes.

It is however critical that the fibers are axially uniform, since axial non-uniformities may give rise to significant sidelobes in the transmission spectrum [17–19]. We therefore investigate to what extent axial variations in acoustooptic phase-mismatch coefficient contribute to the acoustooptic coupling bandwidth in a birefringent two-mode PCF. A method is presented, where axial variations in the acoustooptic phase-mismatch coefficient $\Delta\beta(z)$ are obtained directly from

the transmission spectrum. The method is based on the fact that in the weak coupling regime, there is a Fourier transform relation between the grating parameters (amplitude of the acoustic wave and $\Delta\beta(z)$) and the amplitude and phase of the coupled light. Since the amplitude of the acoustic wave is known (it is approximately constant), one can use the Gerchberg-Saxton algorithm to determine $\Delta\beta(z)$ directly from the measured transmission spectrum. This algorithm transforms successively between the two Fourier domains, fixing the magnitudes at the known values [20,21]. This determines $\Delta\beta(z)$ up to a two-fold ambiguity due to the complex conjugate symmetry of the Fourier transform. This method is compared to an existing method where axial non-uniformities are measured using acoustic pulses [19]. The two methods are found to be in good agreement. The measurements show that the minimum coupling bandwidth is limited by axial variations in acoustooptic phase-mismatch coefficient.

The effect of acoustic birefringence is also investigated. The PCF is found to be acoustically birefringent, and a large contribution to this birefringence is likely due to an unintentional ellipticity of the fiber cross-section.

2. Fiber properties

Optical birefringence in index-guiding photonic crystal fibers can be obtained by introducing a two-fold rotational symmetry into the fiber structure to obtain form birefringence [22–24], or by introducing stress-elements into the cladding to obtain stress-induced birefringence [25]. The fiber used in this experiment is a commercially available PCF of the same type as the one used in Ref. [24], i.e. where two of the air holes on the opposite sides of the core are enlarged to introduce form birefringence. The geometry of the fiber is shown in Fig. 1(a), and a closeup of the core region is shown in Fig. 1(b) and (c). The geometric parameters of the fiber, as obtained from SEM pictures of the fiber cross-section, are $D = 125\ \mu m$ for the fiber diameter, $\Lambda = 4.15\ \mu m$ for the hole spacing, $d_s = 0.50\Lambda$ for the diameter of the small holes, and $d_l = 0.98\Lambda$ for the diameter of the large holes. The experiments are carried out at a wavelength of 633 nm, where the fiber supports four guided modes as schematically shown in Fig. 1(d). The
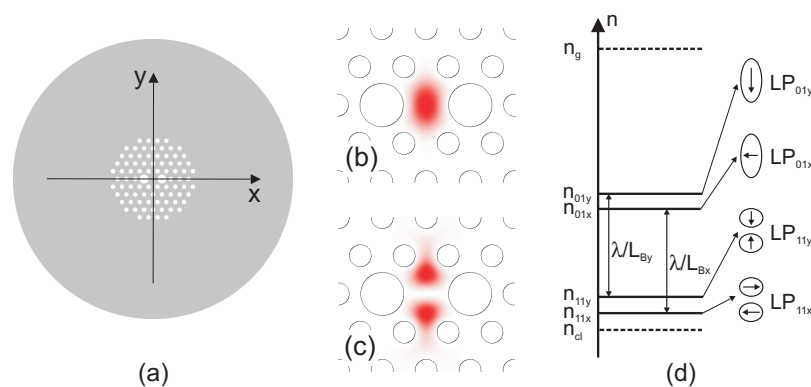
Fig. 1. (a) The birefringent PCF. Calculated intensity profiles of (b) the fundamental modes and (c) the second order modes. (d) Mode diagram. n_g: Refractive index of silica, n_{cl}: Effective cladding index.

four guided modes resemble the two orthogonal polarizations of the LP_{01} and the LP_{11}(even) modes in a standard elliptical-core fiber [16], and are ordered schematically according to their mode index in Fig. 1(d). The splitting in mode index between the two orthogonal polarizations is exaggerated in the figure. It is found that the mode indices of the second order modes are slightly larger than the effective cladding index n_{cl}, which is taken to be to mode index of

the fundamental space-filling mode of the cladding [11]. Both of the two LP_{01} modes have approximately the same intensity distribution, which is shown in Fig. 1(b). In Fig. 1(c), the intensity distribution for the LP_{11} modes is shown. The mode indices and mode profiles are calculated using a fully vectorial solution of Maxwell's equations in a planewave basis [26], using the supercell method [11].

3. Determination of axial variations in acoustooptic phase-mismatch coefficient

Two different methods for determining axial variations in the acoustooptic phase-mismatch coefficient are utilized. We first present a method where $\Delta\beta(z)$ is obtained directly from the transmission spectrum using acoustooptic coupling in a stationary interaction region. We then summarize the basics of an existing method [19], where $\Delta\beta(z)$ is measured using acoustic pulses.
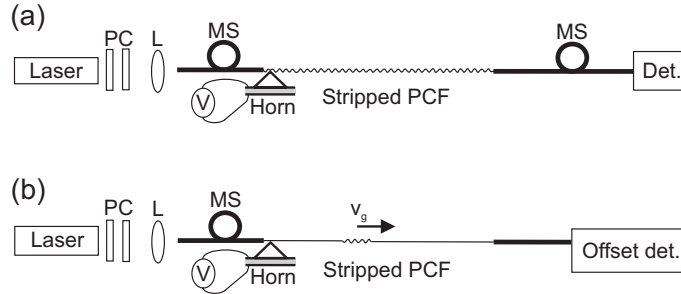
Fig. 2. Experimental setup. (a) Stationary acoustooptic interaction region. (b) Acoustic pulses. PC: Polarization controller, L: Lens, MS: mode stripper.

3.1. Method 1: Stationary acoustooptic interaction region

Consider the setup in Fig. 2(a). Polarized monochromatic light from a laser is coupled into the PCF. A mode stripper ensures that light entering the stripped part of the PCF, i.e. the acousto-optic interaction region, is contained in the LP_{01} modes. The horn generates a continuous flexural acoustic wave of angular frequency Ω_a, which propagates in the stripped PCF section. The frequency and amplitude of the acoustic wave is experimentally controllable. After the stripped PCF section, the light coupled into the second order modes is removed using a second mode stripper, and transmission is recorded as a function of acoustic frequency.

Assuming that the light is linearly polarized along the x- or y-axis of the fiber, the electric field in the stripped PCF section can be represented as a superposition of the (x- or y-polarized) fundamental mode ψ_{01} and second order mode ψ_{11}

$$\psi(\mathbf{r},t) = \sum_{i=01,11} a_i(z)\psi_i(x,y)\exp\left[i\int_{\frac{-L}{2}}^{z}\beta_i(z')\mathrm{d}z'\right]\exp(-i\omega_i t), \tag{1}$$

where the stripped PCF section extends from $z = -L/2$ to $z = L/2$. A scalar notation is used for simplicity and coupling to cladding modes is neglected. Here a_i, ψ_i, β_i, and ω_i denote mode weight, normalized mode profile, propagation constant, and angular frequency, respectively, for mode i. The propagation constants are assumed to depend on z to account for axial non-uniformities, and the angular frequencies satisfy $\omega_{01} = \omega_{11} + \Omega_a$. The mode field evolves

according to the coupled mode equations [27]

$$\frac{\mathrm{d}}{\mathrm{d}z}a_{01}(z) = i\kappa(z)a_{11}(z)\exp\left[-i\int_{\frac{-L}{2}}^{z}\Delta\beta(z',\Omega_a)\mathrm{d}z'\right]$$ (2)

$$\frac{\mathrm{d}}{\mathrm{d}z}a_{11}(z) = i\kappa^*(z)a_{01}(z)\exp\left[i\int_{\frac{-L}{2}}^{z}\Delta\beta(z',\Omega_a)\mathrm{d}z'\right],$$ (3)

where the acoustooptic phase-mismatch coefficient is given by

$$\Delta\beta(z,\Omega_a) = \beta_{01}(z) - \beta_{11}(z) - K_a(z,\Omega_a),$$ (4)

and K_a is the wavenumber of the acoustic wave. $\kappa(z)$ is the acoustooptic coupling constant, which is proportional to the amplitude of the acoustic wave. Note that a_i also depends on Ω_a, but this has been suppressed in the notation for simplicity. We then assume that $\kappa(z) = \kappa$, that is, damping of the acoustic wave along the acoustooptic interaction region is neglected. We also assume that

$$\Delta\beta(z,\Omega_a) = \Delta\beta(z,\Omega_0) + \Delta\tilde{\beta}(\Omega_a) \equiv \Delta\beta(z) + \Delta\tilde{\beta}(\Omega_a),$$ (5)

where the first term represents the variation in $\Delta\beta$ due to axial non-uniformities, at the angular frequency Ω_0, and the second term refers to variations in $\Delta\beta$ with acoustic frequency for a perfect, axially uniform structure. The validity of an assumption similar to Eq. (5) has been discussed in Ref. [19]. It is assumed that $a_{11}(-L/2) = 0$, and that the amplitude of the acoustic wave is sufficiently low, such that $a_{01}(z) \approx a_{01}(-L/2) = 1$. We then obtain

$$\frac{\mathrm{d}}{\mathrm{d}z}a_{11}(z) = i\kappa^*\exp\left[i\int_{\frac{-L}{2}}^{z}\Delta\beta(z')\mathrm{d}z'\right]\exp\left[i\Delta\tilde{\beta}(\Omega_a)(z+L/2)\right].$$ (6)

It is then assumed that

$$\Delta\tilde{\beta}(\Omega_a) \approx \frac{\mathrm{d}\Delta\tilde{\beta}(\Omega_0)}{\mathrm{d}\Omega_a}(\Omega_a - \Omega_0) \approx -\frac{\mathrm{d}K(\Omega_0)}{\mathrm{d}\Omega_a}\Delta\Omega = -\frac{\Delta\Omega}{v_g(\Omega_0)},$$ (7)

where v_g is the acoustic group velocity, and $\Delta\Omega = \Omega_a - \Omega_0$. Defining $\phi(z) = \int_{-L/2}^{z}\Delta\beta(z')\mathrm{d}z'$ and $u(\Omega_a) = -ia_{11}(L/2)\exp[-i\Delta\tilde{\beta}(\Omega_a)L/2]/\kappa^*$, we obtain

$$u(\Omega_a) = \int_{-\infty}^{\infty} h(z)\exp\left[-i\Delta\Omega z/v_g(\Omega_0)\right]\mathrm{d}z,$$ (8)

where we have defined

$$h(z) = \begin{cases} \exp\left[i\phi(z)\right] & \text{if } \frac{-L}{2} \leq z < \frac{L}{2} \\ 0 & \text{otherwise.} \end{cases}$$ (9)

In other words, $u(\Omega_a)$, which is proportional to the amplitude of the coupled light, is the Fourier transform of $h(z)$, which describes the grating. This means that if we know $u(\Omega_a)$, we can use the inverse Fourier transform to determine $h(z)$ and thereby find $\Delta\beta(z)$ using

$$\Delta\beta(z) = \frac{\mathrm{d}}{\mathrm{d}z}\phi(z).$$ (10)

The problem is that experimentally, when the transmission spectrum is recorded, only $|u(\Omega_a)|$ is obtained. However, since $|h(z)|$ is known, the Gerchberg-Saxton (G-S) algorithm can be used to find $\phi(z)$. The algorithm works as follows [20]:

1. The initial values of $\phi(z)$ are chosen randomly in the interval $-\pi \ldots \pi$.

2. The Fourier transform (FFT) of $h(z)$ is computed.

3. The computed phase of u is combined with the known value of $|u|$ and the inverse Fourier transform (IFFT) is computed

4. The new values for $\phi(z)$ are used as input to the algorithm, and step (2)-(4) are repeated until convergence.

Convergence is checked by comparing the measured $|u|$ with the one computed from h using $\phi(z)$ determined by the G-S algorithm. A two-fold ambiguity does however arise since $|h(z)|$ is symmetric [21]. This is due to the fact that the complex conjugate symmetry of the Fourier transform causes both $\phi(z)$ and $-\phi(-z)$ to give the same $|u|$. It cannot be determined which of these two solutions are found by the G-S algorithm. Despite this shortcoming, the G-S method is useful due to its experimental and computational simplicity.

3.2. Method 2: Acoustic pulses

Consider the case where the acoustic horn generates a pulse of duration t_a with carrier frequency $\Omega_a/(2\pi)$. The acoustic pulse will travel along the stripped part of the fiber with group velocity $v_g(\Omega_a)$, as shown in Fig. 2(b), and the length of the pulse is $l_p = v_g t_a$. The acoustic pulse therefore acts as a long-period grating with length l_p, moving along the stripped part of the PCF with velocity v_g. In Ref. [19] it was shown that $\Delta\beta(z)$ is given by

$$\Delta\beta(z) = \frac{\Omega(z/v_g) - \Omega_a}{v_g}, \tag{11}$$

where $\Omega(z/v_g)$ is the frequency shift of the coupled light at a pulse position $z = -L/2 + v_g t$. Hence, by measuring the beat frequency between the modes ψ_{01} and ψ_{11} as a function of time, one obtains $\Delta\beta(z)$. Note that the frequency spectrum of the acoustic pulse must contain the frequency range of $\Omega(z/v_g)$ for this method to work. This can achieved by choosing a short pulse (with a corresponding wide frequency spectrum), and choosing Ω_a close to the expected range of $\Omega(z/v_g)$.

4. Results and discussion

A 48 cm section, denoted section 1, of the PCF was stripped to allow for propagation of the acoustic wave. The acoustic horn was a hollow aluminum cone filled with epoxy. It was optimized for having a broad frequency response [28], whose magnitude was found to be approximately constant in the frequency range of interest. The horn was made in contact with the stripped PCF section using a drop of silicone oil. This made it possible to rotate the acousto-optic interaction region with respect to the horn tip. Each mode stripper was made by coiling the PCF 5 turns around a post with a diameter of 5 mm. This effectively removed the light in the second order modes due to the high macrobending loss of the second order modes, compared to the fundamental modes.

Using the setup in Fig. 2(a) as a starting point, the second mode stripper and the detector was removed and a CCD array was placed 8 mm from the fiber end. The light polarization and fiber orientation was varied, and it was found that the acoustic wave coupled light from the LP_{01} to the LP_{11} modes, with negligible coupling to cladding modes in the relevant frequency range. By optimizing the position of the horn tip, the light polarization, and the fiber orientation, we were able to couple more than 90% of the light from the LP_{01} to the LP_{11} mode at an acoustic frequency of 7.379 MHz. An example of the measured mode profile with the acoustic wave on/off is shown in Fig. 3.

<div align="center">(a)   (b)</div>
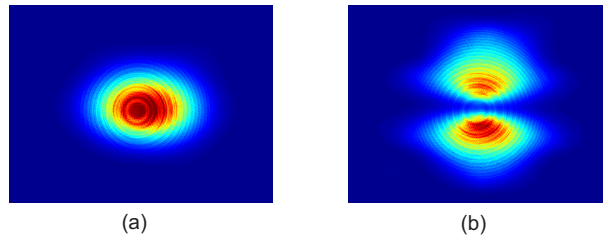
Fig. 3. Measured mode profile for (a) acoustic wave *off* and (b) acoustic wave *on*.

4.1. Acoustic birefringence

It is clear from Fig. 1(a) that for a perfect fiber, the *x*- and *y*-polarized flexural acoustic waves will have different propagation constants due to the two-fold rotational symmetry of the fiber cross-section. It has however previously been shown for a Hi-Bi fiber that an unwanted ellipticity in the fiber cross-section can constitute the main contribution to the acoustic birefringence, and that the acoustic axes therefore not necessarily coincide with the *x*- and *y*-axis [29].

Using acoustic pulses, the effect of acoustic birefringence was studied for the PCF. The setup for characterizing the PCF using acoustic pulses is shown in Fig. 2(b). As discussed in Sec. 3.2, the acoustic pulse acts as a long period grating of length l_p moving at a speed v_g. The frequency shift of the coupled light is related to $\Delta\beta(z)$ according to Eq. (11).

The frequency shift of the coupled light was measured as a function of time using an offset detector and a digital oscilloscope. Each point in time corresponds to a given pulse position as the pulse travels along the stripped PCF. The acoustic pulse was a square wave with a carrier frequency of 7.4 MHz. The duration of the pulse was $t_a = 2.7\ \mu$s, corresponding to a frequency spectrum of width $\Delta f \approx 1/t_a = 0.37$ MHz. Using a laser probing technique [3], an acoustic group velocity of $v_g = 3516$ m/s was measured at 7.4 MHz. This gives a pulse length $l_p = v_g t_a = 9.5$ mm.

We denote linearly polarized light along the *x*- and *y*-axis as opt. pol. 1 and opt. pol. 2, respectively. The acoustic axes are denoted as the x'- and y'-axis, and the corresponding polarizations of the flexural acoustic wave are called ac. pol. 1 and ac. pol. 2. Figure 4(a) shows a recorded interferogram using ac. pol. 2 and opt. pol. 1. The frequency shift of the coupled light is approximately 7.4 MHz, resulting in a signal period close to 0.5 mm. The polarization of the light was then optimized to excite an equal amount of opt. pol. 1 and opt. pol. 2. Using the identity $\cos(k_1 z) + \cos(k_2 z) = 2\cos[(k_1 - k_2)z/2]\cos[(k_1 + k_2)z/2]$, we find that the slowly varying envelope in Fig. 4(b) is given by $\cos[(\Delta\beta_x - \Delta\beta_y)z/2]$, where $\Delta\beta_x = 2\pi(n_{01x} - n_{11x})/\lambda$ and $\Delta\beta_y = 2\pi(n_{01y} - n_{11y})/\lambda$. From Fig. 4(b) one then obtains $|\Delta\beta_x - \Delta\beta_y| = 2\pi/L_{z1} \approx 114\ \text{m}^{-1}$, where $L_{z1} \approx 5.5$ cm is the distance between two zeros of the slowly varying envelope.

Figure 4(c) shows the resulting interferogram using ac. pol. 2 and opt. pol 2, and is similar to Fig. 4(a), except for a small change in the signal period since $\Delta\beta_x \neq \Delta\beta_y$. In Fig. 4(d) the stripped part of the PCF was rotated an angle of $70°$, compared to Fig. 4 (a), to excite a combination of ac. pol. 1 and ac. pol. 2. The optical polarization was opt. pol. 1. The rotation angle of the stripped PCF section was chosen such that both the x' and the y' component of the acoustic wave contributed equally to the acoustooptic coupling coefficient. This can be used to determine the angle between the acoustic and optical axes [29]. Using the method in Ref. [29], we estimate that this angle is approximately $20°$ in this PCF section. From the distance $L_{z2} \approx 28.0$ cm between the zeros in the slowly varying envelope, it is found that $|K_1 - K_2| = 2\pi/L_{z2} \approx 22.4\ \text{m}^{-1}$, where K_1 and K_2 are the propagation constants for ac. pol. 1 and ac. pol. 2, respectively. An
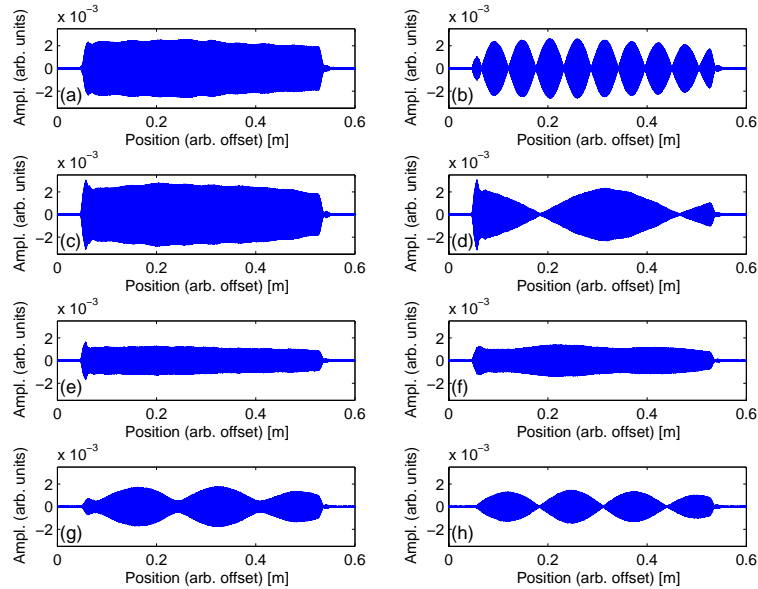
Fig. 4. Interferograms. (a) Ac. pol. 2, opt. pol. 1. (b) Ac. pol. 2, opt. pol. 1 and 2. (c) Ac. pol. 2, opt. pol. 2. (d) Ac. pol. 1 and 2, opt. pol. 1. (e) Ac. pol. 1, opt. pol. 1. (f) A $180°$ twist of the AO-region. (g) A $360°$ twist of the AO-region. (h) A $540°$ twist of the AO-region.

unintentional ellipticity in the fiber cross-section of the order of 10^{-3} is estimated to be sufficient to account for the measured acoustic birefringence. Figure 4(e) shows the interferogram obtained using ac. pol. 1 and opt. pol. 1. This was achieved by rotating the acoustooptic interaction region an angle of $90°$ compared to Fig. 4(a), and demonstrates experimentally that the x'- and y'-axis are orthogonal.

We then used ac. pol. 2 and opt. pol. 2 as a starting point, and fixed the orientation of the fiber at the horn. The orientation of the other end of the acoustooptic interaction region was rotated in steps of $180°$, and an interferogram was recorded at each step. Figure 4(f)-(h) shows the resulting interferogram for a twist angle θ of $180°$, $360°$, and $540°$, respectively. For higher twist angles the interferograms are similar to Fig. 4(h), except for n zeros in the the envelope for a $n \cdot 180°$ twist. This is interpreted as when $\theta \geq 540°$, the polarization of the acoustic wave is not able to follow the twist, but remains approximately constant with respect to the laboratory frame along the entire acoustooptic interaction region. For pulse positions where the polarization of the acoustic wave is orthogonal to the y-axis, the acoustooptic coupling constant is zero due to symmetry, resulting in zeros in the slowly varying envelope of the interferogram [30]. Since such zeros are not observed for $\theta = 180°, 360°$, the acoustic polarization is affected by weak twists of the fiber. It can be noted that in the limit of strong acoustic birefringence, the acoustic polarization should be able to follow the twist, in the same manner as the optical x- or y-polarization follows the twist of the birefringent PCF, which then should have no influence on the interferogram.

4.2. *Axial variations in acoustooptic phase-mismatch coefficient*

We here report results using method 1 and method 2 to measure axial variations in the acoustooptic phase-mismatch coefficient. The four upper curves in Fig. 5(a) shows measured transmission in section 1 as a function of frequency for all four combinations of acoustic and optical
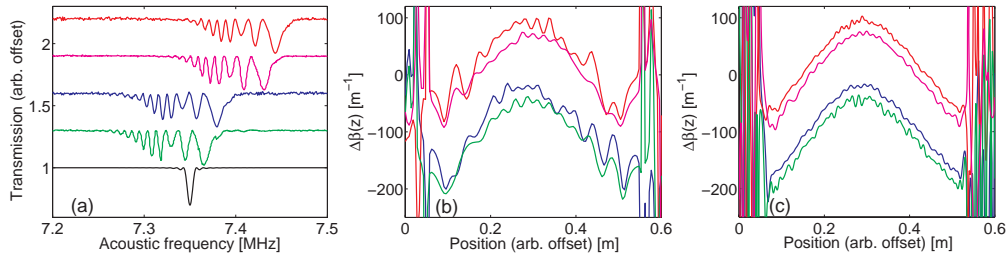
Fig. 5. (a) Measured transmission in section 1. (b) Retrieved $\Delta\beta(z)$ using the G-S algorithm. (c) Retrieved $\Delta\beta(z)$ using acoustic pulses. Red curves: Ac. pol 2, opt. pol. 2. Magenta curves: Ac. pol. 1, opt. pol. 2. Blue curves: Ac. pol. 2, opt. pol. 1. Green curves: Ac. pol. 1, opt. pol. 1. Black curve: Ideal computed transmission for an axially uniform fiber.

polarizations. Also shown is an ideal transmission spectrum for an axially uniform fiber, i.e. when $\Delta\beta(z)$ is constant (black curve). It is apparent that axial non-uniformities dominate the coupling bandwidth (coupling to other modes has been ruled out experimentally using the CCD camera). The measured transmission spectrum is used as an input to the G-S algorithm and $\Delta\beta(z)$ is determined, as shown in Fig. 5(b). As noted above, the algorithm yields either $\Delta\beta(z)$ or $\Delta\beta(-z)$, and one cannot determine which of the two solutions is the correct one. Only one of the two solutions is shown in the figure (Accidentally, $\Delta\beta(z) \approx \Delta\beta(-z)$ in this fiber section, so the two solutions are almost similar). As a reference measurement we determined $\Delta\beta(z)$ using acoustic pulses as shown in Fig. 5(c). By comparing Fig. 5(b) and (c) we observe that the two methods are in reasonable agreement. Note that $\Delta\beta(z)$ is undefined outside the coupling region. This shows up as noise in the measurements. It is clear from Fig. 5 that the axial variation in $\Delta\beta(z)$ is the same for all four combinations of acoustic and optical polarizations. A possible cause for this is that the fiber diameter might vary with z. An experimental characterization of the fiber diameter is left for future studies.
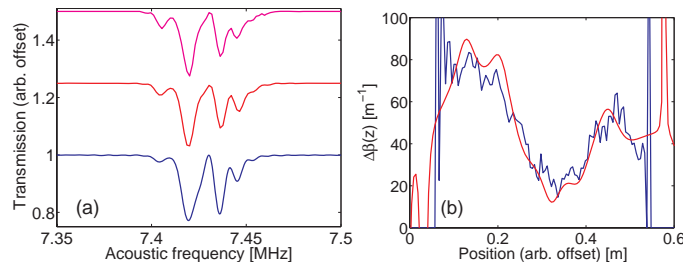
Fig. 6. (a) Measured transmission in section 2 (magenta curve), computed transmission using $\Delta\beta(z)$ found by the G-S method (red curve) and by acoustic pulses (blue curve). (b) Retrieved $\Delta\beta(z)$ in section 2 using the G-S algorithm (red curve) and acoustic pulses (blue curve).

The measurements were repeated for a different fiber section, denoted section 2, using ac. pol. 1 and opt. pol. 1. The results are reported in Fig. 6(a) and (b). The upper solid line in Fig. 6(a) shows measured transmission in section 2. Outside a 0.07 MHz bandwidth, the acoustooptic coupling was negligible, and the measured transmission has been set to 1 to remove noise in the G-S algorithm. Figure 6(b) shows retrieved $\Delta\beta(z)$ using the G-S algorithm (red curve) and acoustic pulses (blue curve). As a consistency check, the retrieved $\Delta\beta(z)$ is used to calculate the transmission spectrum, as shown in Fig. 6(a), using $\Delta\beta(z)$ determined by the G-S method (red

curve) and acoustic pulses (blue curve). Both methods reproduce the measured transmission spectrum very well, as shown in the figure.

5. Conclusion

The aim of this work is to investigate how fiber imperfections affect the coupling bandwidth of an acoustooptic tunable filter based on a two-mode index-guiding birefringent PCF, where the optical birefringence is due to two enlarged air holes on the opposite sides of the core.

The PCF is found to be acoustically birefringent. A large contribution to this birefringence is likely due to an unintentional ellipticity of the fiber cross-section.

The two methods for determining axial variations in acoustooptic phase-mismatch coefficient are seen to be in good agreement. The G-S approach is experimentally and computationally simple, but yields a two-fold ambiguity in $\Delta\beta(z)$. Using acoustic pulses is experimentally more complex, but the two-fold ambiguity in $\Delta\beta(z)$ is avoided. For the fiber investigated it is found that the minimum acoustooptic coupling bandwidth is limited by axial variations in acoustooptic phase-mismatch coefficient.

Acknowledgment